energies

MDPI

Article

An Optimal Train Speed Profile Planning Method for Induction Motor Traction System

Ziyu Wu [1,2,3,*], Chunhai Gao [2,3] and Tao Tang [1]

[1] School of Electronics and Information Engineering, Beijing Jiaotong University, Beijing 100044, China; ttang@bjtu.edu.cn
[2] Traffic Control Technology Co., Ltd., Beijing 100070, China; chunhai.gao@bj-tct.com
[3] National Engineering Laboratory for Urban Rail Transit Communication and Operation Control, Beijing 100044, China
* Correspondence: wuzyca@126.com

Abstract: Optimizing the operating speed curve of trains without adding new energy storage facilities is essential in the energy-saving operation of railways. In this paper, we propose an optimal train speed curve planning method for driving trains more energy efficiently. A refined traction energy evaluation model for induction motor propulsion systems is first presented. The proposed model considers the efficiency of the traction motor at different operating points and the efficiency of the inverter and gearbox. Then, the optimal energy-efficient speed profile problem is transformed into a multistep decision problem and solved using dynamic programming (DP). To verify the effectiveness of the proposed method, a case study was conducted on an actual subway line. The results obtained indicate that the speed curve produced by the proposed method results in a 20% energy consumption saving compared with the speed curve for actual operations. Furthermore, the results of comparison with a genetic algorithm indicate that the DP algorithm is better able to satisfy the constraints of the train traction system. Solving the optimal speed curve using the proposed method and programming the onboard controller of the train according to the optimal speed curve enables the train to be driven with greater energy efficiency.

Keywords: energy efficiency; dynamic programming; train speed profile; induction motor; traction system

Citation: Wu, Z.; Gao, C.; Tang, T. An Optimal Train Speed Profile Planning Method for Induction Motor Traction System. *Energies* **2021**, *14*, 5153. https://doi.org/10.3390/en14165153

Academic Editors: Calin Iclodean and Daniel Morinigo-Sotelo

Received: 8 July 2021
Accepted: 17 August 2021
Published: 20 August 2021

1. Introduction

The electrified railway system has many advantages, such as high capacity, low emissions, and enhanced performance. The energy consumption of a railway system per transported passenger is much lower than that of any road-bound transport [1]. As the transport sector is responsible for approximately 23% of global CO_2 emissions [2], it is important to operate trains efficiently [3]. The EU co-funded railway project "MyRailS" is engaged in reducing energy consumption and CO_2 emissions to develop sustainable railway systems [4,5].

Technologies for energy-efficient railway systems have been researched for several decades [6–9]. The energy-saving operation of railways relies on technological advancements in many fields, including the development of train propulsion systems [10], advances in train traction power supply systems [11–13], and advanced train dispatch and driving technology [14–16].

As vehicle traction energy consumption accounts for a relatively high proportion of railway operation energy consumption, many scholars have investigated ways to reduce vehicle traction energy consumption [17]. Zarifyan et al. [18] developed an algorithm that ensures the energy efficiency of the electric locomotive by regulating the number of traction motors (TMs). Liubarskyi et al. [19] quantified the instantaneous electrical losses of the traction drive for a permanent magnet synchronous motor (PMSM) and optimized the

traction drive for maximum efficiency. Serhiy et al. [20] studied the optimal design for the electric transmission traction of a shunting locomotive. In addition to improving the TM and drive efficiency, the recovery and utilization of train electrical braking energy can also achieve energy-saving effects [21].

Several scholars have attempted to achieve energy savings by optimizing train schedules and driving strategies under the conditions of existing railway facilities. Yang et al. [22] proposed an energy-efficient rescheduling approach under delay perturbations. Their proposed method achieved an 8.19% net energy reduction in comparison with the traditional approach. Tian et al. [23] developed a smart drive package and advanced tram and train trajectory optimization techniques based on dynamic programming (DP). The results of field trials carried out on the Edinburgh Tram Line in the UK indicated energy savings of 10–20%. Li et al. [24] completed an optimization energy-efficient trajectory based on a genetic algorithm (GA) for driver advisory systems (DAS) and proposed an online punctuality adjustment system. Wang et al. [25] formulated train trajectory optimization as a multiple-phase optimal control problem and solved it using a pseudo-spectral method. Huang et al. [26] described the relationship between the energy consumption of urban rail transit systems and speed profile using machine learning algorithms.

From the current research, it is clear that optimizing the train operation curves results in energy-saving effects. However, existing methods ignore the changes in the efficiency of the TM at different points of operation and set the efficiency of the TM to a fixed value over certain sections when the train operation curve is planned. This simplified method may cause the planned speed curve to deviate from the best efficiency of the TM at the operating point, resulting in greater energy losses by the motor. In response to this problem, some scholars have tried combining speed planning with refined motor efficiency models. The losses of the propulsion system at exact points are calculated using software based on a physical model developed by Bombardier [27]. However, a large amount of test data and model tuning work are required to build the physical model and obtain the losses at different work points. The dynamic loss of a traction system is obtained using the mathematical model of the PMSM in the d–q axis coordinate system [28]. Nevertheless, the currents and voltages in the d–q axis must be calculated at each time step.

Unlike the models presented in the literature, the approach proposed in this paper considers the dynamic efficiency of the train TM to plan the speed curves, which makes the energy consumption model more economical. In particular, the induction motor (IM) equivalent circuit model (ECM) is used to calculate the efficiency of the motor at specific operating points offline, which reduces the complexity of the calculation and the requirements for measurement data. In addition, other essential aspects, such as air resistance, gradient force, comfort constraints, maximum acceleration, and different maximum speed limits are considered when the speed curve is planned.

The main contributions of this study are as follows: (i) the development of a new model that captures motor efficiency and traction energy consumption more accurately; (ii) the development of an optimal model for solving the most energy-efficient speed profile based on DP; and (iii) the implementation of our solution to estimate the energy reduction obtained for real urban rail transit line examples.

The remainder of this paper is organized as follows. In Section 2, a dynamic energy consumption model for train electric traction systems is introduced. Section 3 presents the optimal energy-saving train speed curve model based on DP. A case study carried out on a metro railway line in Shijiazhuang is discussed in Section 4. Finally, the conclusion and ongoing research are discussed in Section 5.

2. Electric Traction System Energy Consumption Model

Electric multiple unit (EMU) trains are popular for urban rail transit worldwide because of their fast acceleration and pollution-free operation [29]. The cars that form a complete EMU set can usually be separated by function into the following four types: power cars, motor cars, driving cars, and trailer cars. Driving cars are at the outer ends of

an EMU, containing a driver's cab or an automatic train operation (ATO) unit. Motor cars carry TMs to move the train and are often combined with a power car. The traction system is installed in the motor car, which mainly contains TMs, gearboxes, inverters, and bogies, as shown in Figure 1.

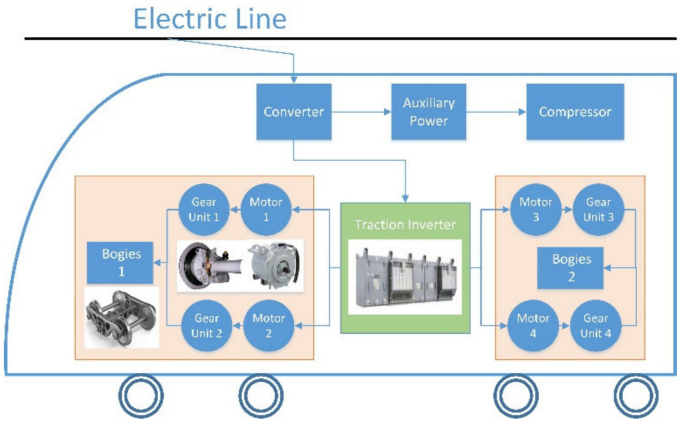

Figure 1. Schematic of a motor car.

As shown in Figure 1, the power flows from the substation to the motor car converter through the electric line. Inside the vehicle, there are two main types of equipment that consume electrical energy. One kind is the auxiliary systems, such as for air conditioning and lighting, and the other is the traction propulsion system. Most EMU trains are operated in vehicle mode, which controls four motors using one inverter.

2.1. Train Dynamic Model

To simplify the calculation, a single mass point model is used to describe the movement of the train. A schematic of train force analysis is shown in Figure 2 that assumes that the mass of the train is concentrated at mass point CG.

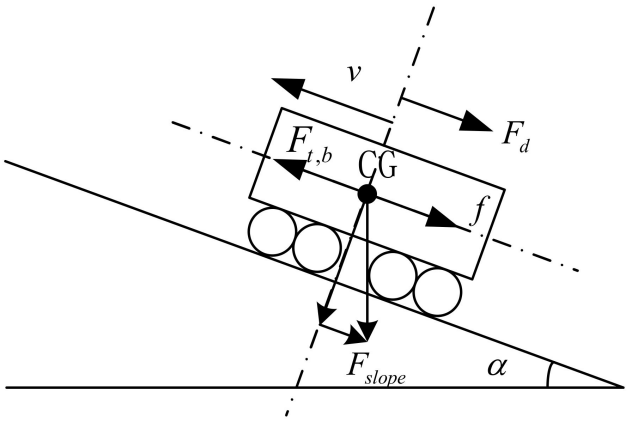

Figure 2. Schematic of train force analysis.

The train motion equation can be described as follows:

$$m\dot{v}_x = N_m F_t(u, v) - F_d(v) - f \tag{1}$$

where m is the mass of the train and passengers; F_t is the traction/braking force generated by one power axle; v is the speed of the train; N_m is the number of power axles; F_d is the Davis equation representing the running resistance, which includes air resistance and

mechanical resistance, as described in Equation (2); and f is the additional resistance of the line, as described in Equation (3) as follows:

$$F_d = a + bv + cv^2 \tag{2}$$

$$f = mg\sin\alpha + \frac{A}{R_L} \tag{3}$$

where α is the line gradient; a, b, and c are the coefficients for the running resistance of the train and can be measured via an idle test; A/R_L represents the additional resistance caused by the bending of the line; A is the line curve resistance coefficient, for which the value can be found from the standard TB/T 1407-1998; and R_L is the line radius.

The power wheels are connected to the gearbox through the axles. A schematic of the wheel axle is shown in Figure 3.

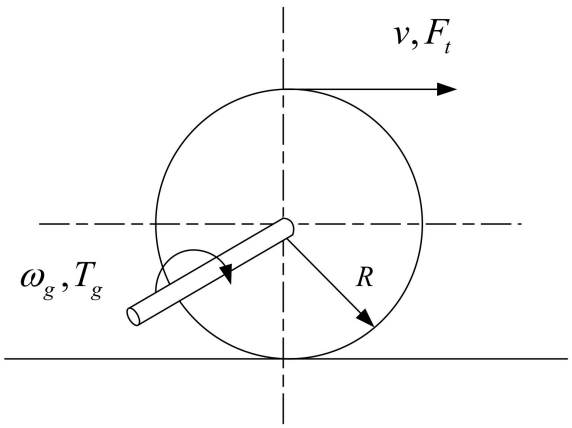

Figure 3. Diagram of the power wheel and axle.

Assuming that the wheels do not slip, the dynamic model of the wheel and axle can be expressed as follows:

$$F_t = \frac{T_g}{R} \tag{4}$$

$$v = R\omega_g \tag{5}$$

where ω_g and T_g are the output mechanical rotational speed and torque of the axle, respectively, and R is the wheel radius.

The gearbox represents the fixed gear ratio transmission equipment. The following equations describe the relationship between the input and output physical quantities of the gearbox:

$$\omega_s = i_g\omega_g \tag{6}$$

$$P_s = \omega_s T_s \tag{7}$$

$$P_g = \omega_g T_g = \eta_g P_s \tag{8}$$

where ω_s, T_s, and P_s are the angular velocity, torque, and power of the gearbox input port, respectively; i_g and η_g are the transmission ratio and efficiency of the gearbox, respectively; and ω_g, T_g, and P_g are the angular velocity, torque, and power of the output port, respectively.

2.2. Induction Motor Model

Owing to their simple structure and high torque, AC induction motors are widely used in EMU trains. A T-type ECM is introduced to describe the asynchronous IM, as shown in Figure 4.

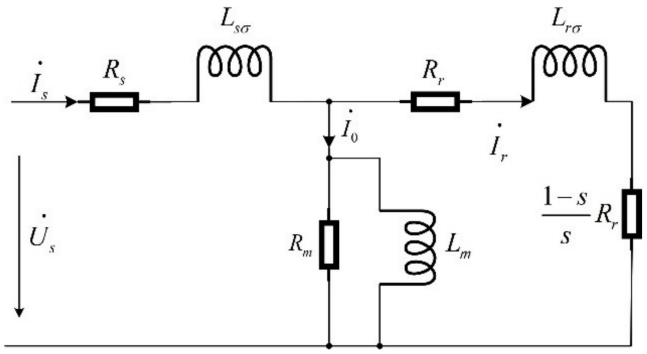

Figure 4. T-type equivalent circuit model (ECM) of an induction motor.

In Figure 4, I_s, I_0, and I_r represent the input current, excitation current, and rotor current, respectively. $L_{s\sigma}$, $L_{r\sigma}$, and L_m are the leakage inductances of the stator, rotor, and magnetizing inductance, respectively; s is the slip ratio; R_r is the rotor equivalent resistance; R_s is the stator resistance; and R_m is the equivalent resistance of the exciting branch. The parameters of the IM equivalent circuit and its magnetization inductance curve can be obtained through no-load and short-circuit tests of the motor following IEC Standard 60034-28.

The total mechanical power generated by the motor through electromagnetic induction can be expressed as follows:

$$P_{mec} = m_2 I_r^2 \frac{1-s}{s} R_r \tag{9}$$

where m_2 is the phase number of the motor. The output power of the motor is as follows:

$$P_2 = P_{mec} - p_m \tag{10}$$

where p_m represents the mechanical and additional loss of the motor and can be valued according to IEC Standard 60034-2. The output torque is as follows:

$$T_m = \frac{P_2}{\omega_m} \tag{11}$$

The motor active input power is as follows:

$$P_1 = m_2 U_1 I_1 \cos\varphi \tag{12}$$

where φ is the power factor. The efficiency of the motor can be calculated as follows:

$$\eta_m = \frac{P_2}{P_1} \tag{13}$$

As the source port of the gearbox is connected to the output shaft of the TM, the relationship between the physical quantities of the gearbox and motor can be expressed as follows:

$$P_2 = P_s \tag{14}$$

$$\omega_m = \omega_s \tag{15}$$

2.3. Train Traction Energy-Cost Model

When the train accelerates, the electric energy must be absorbed from the catenary. The motor converts electrical energy into mechanical power, which is transmitted to the wheel through the gearbox and axle. Therefore, in this study, the amount of electric energy absorbed by the traction inverter from the catenary is defined as the train traction energy consumption.

The traction power can be evaluated using the following:

$$p = \frac{N_m F_t v}{\eta_g \eta_i \eta_m} \tag{16}$$

where η_i is the efficiency of the inverter and p is the traction power of the train. Although the motor generates energy during braking, the braking energy recovery requires the installation of energy storage equipment; therefore, the braking energy is not considered.

The efficiency of the gearbox and inverter varies minimally throughout the operating range, and they can be set as constants. However, because the efficiency of the TM fluctuates significantly with the change in the operating point (v, F_t), it is necessary to acquire a motor efficiency table corresponding to the operating points of the train to obtain an accurate measurement of traction energy consumption.

In this study, to obtain the relationship between motor efficiency η_m and operating point (v, F_t), an ECM-based method is proposed. First, by changing the amplitudes and frequencies of $\dot{U}_s$ in the ECM, as shown in Figure 4, a steady-state model of the motor corresponding to different operating points can be obtained.

Assuming that the slip ratio is the rated slip rate, the relationship between the $\dot{U}_s$ frequency and the mechanical angular velocity can be expressed as follows:

$$\omega_m = \frac{2\pi(1-s)f_s}{P_m} \tag{17}$$

where P_m is the number of motor pole pairs, and f_s is the frequency of $\dot{U}_s$. From Equation (17), it can be observed that the mechanical angular velocity ω_m is proportional to the frequency of $\dot{U}_s$. As I_r is proportional to the amplitude of $\dot{U}_s$, it can be noted from Equations (10) and (11) that the output mechanical power P_2 is approximately proportional to u_s^2.

After the frequency and amplitude of $\dot{U}_s$ are given, the voltage and current of each branch in the ECM can be solved using Kirchhoff's law. By using Equations (10)–(13), the motor efficiency table for $\eta_m(\omega_m, P_2)$ can be obtained. By using Equations (4)–(8), the table for $\eta_m(\omega_m, P_2)$ can be converted to a table for $\eta_m(v, F_t)$. The motor efficiency at any operating point can be calculated using the bilinear interpolation method according to the table for $\eta_m(v, F_t)$. As the parameters of the ECM are easy to measure relative to the traditional method of testing the efficiency in an actual motor, this method can accurately obtain the efficiency of the motor at any operating point. Correspondingly, the traction power can be calculated using Equation (16).

3. Dynamic Program

After obtaining the traction power of the train, the optimal energy-cost speed curve plan problem can be expressed as follows:

$$\min J = \int_0^T p(t)dt \tag{18}$$

$$subj: \begin{cases} v(s) < v_{\max}(s) \\ F_{b\max}(v) < F_t(v) < F_{t\max}(v) \\ a_{\min} < \dot{v}(s) < a_{\max} \end{cases} \tag{19}$$

where T is the train travel time; $v_{max}(s)$ is the line limit speed at position s; F_{tmax} and F_{bmax} are the maximum traction force and braking force generated by the motor at speed v, respectively; and a_{min} and a_{max} are the minimum and maximum accelerations, respectively, considering passenger comfort requirements.

The model defined in Equations (1), (18), and (19) can be solved using DP as defined by Bellman in the 1950s. It is necessary to transform the original problem into a multistage decision process. The speed curve planning problem is transformed into solving for the

train position and corresponding speed in each decision stage. Therefore, discrete positions and speeds comprise the state variable, which is defined as $x_k = [s_k\ v_k]$. The train motion model (1) is discretized and can be expressed as follows:

$$v_{k+1} = v_k + \frac{u_k - F_d^k - f_k}{m}\Delta t \tag{20}$$

$$s_{k+1} = s_k + \frac{v_k + v_{k+1}}{2}\Delta t \tag{21}$$

where $u_k = F_{t,b}^k$ is the control variable applied to the state variable, x_k. The control variables are a given number of levels of maximum tractive/braking effort. Δt is a discrete step in the time domain. The number of divisions is N. The time step can be expressed as follows:

$$\Delta t = \frac{T}{N} \tag{22}$$

The transition cost from state x_k to x_{k+1} under the control of u_k can be expressed as follows:

$$\phi_k = p^k \times \Delta t = \begin{cases} \dfrac{N_m u_k (v_k + v_{k+1})}{2\eta_g \eta_i \eta_m}\Delta t, if u_k > 0 \\ 0, if u_k \le 0 \end{cases} \tag{23}$$

where p^k is the traction power of the control force u_k at state x_k. If the state violates the constraints of Equation (19), the transition cost is set to a large value ϕ_m and can be expressed as follows:

$$\phi_m = F_{t\max} v_{\max} T \tag{24}$$

The terminal cost is defined as follows:

$$\phi_N = \lambda_1(s(T) - L) + \lambda_2(v(T)) \tag{25}$$

where L is the desired travel distance and λ_1 and λ_2 are the penalty coefficients of the distance and velocity, respectively. The terminal cost is the penalty for a terminal state that deviates from the target state.

The cost at step k can be described as follows:

$$J_k = J_{k-1} + \phi_k \tag{26}$$

The original problem of Equation (17) can be expressed as follows:

$$\min_{u_k = \{u_1, u_2, \cdots u_{N-1}\}} \left\{ \sum_{k=1}^{N-1} \phi_k(x_k, u_k) + \phi_N(x_N, u_N) \right\} \tag{27}$$

By using the backward search and bilinear interpolation algorithm proposed by Kristianingtyas and Miyatake [28], the optimal control inputs at every state lattice point can be solved. The train speed profile can be obtained by using the optimal control inputs to search forward.

4. Case Study

To validate the effectiveness of the proposed method, Metro Line 3 of Shijiazhuang was chosen for the case study. The train set is formulated by 4M2T, where M represents the motor vehicle and T represents the trailer vehicle. The train parameters are listed in Table 1.

Considering that the magnetic field of the motor is saturated, the magnetizing inductance value gradually decreases as the air-gap magnetic density increases. The variation in the magnetizing inductance with the input voltage is shown in Figure 5.

Table 1. Train parameters.

Parameter	Symbol	Value	Unit
Mass at AW0	m	222	ton
Radius of wheel	R	0.42	m
Gear ratio	i_g	6.6875	/
Gearbox efficiency	η_g	0.98	/
Inverter efficiency	η_i	0.97	/
Maximum acceleration	a_{max}	1.0	m/s^2
Minimal acceleration	a_{min}	−1.0	m/s^2
Maximum velocity	V_{max}	22.22	m/s
Number of motors	N_m	16	/
Number motor pole pairs	P_m	2	/
Slip ratio	s	0.0495	/
Stator resistor	R_s	51.5	mΩ
Rotor resistor	R_r	29.7	mΩ
Excitation resistor	R_m	160	Ω
Stator inductance	L_s	0.923	mH
Rotor inductance	L_r	0.563	mH
Magnetizing inductance	L_m	26.372	mH
Additional loss	p_m	300	w

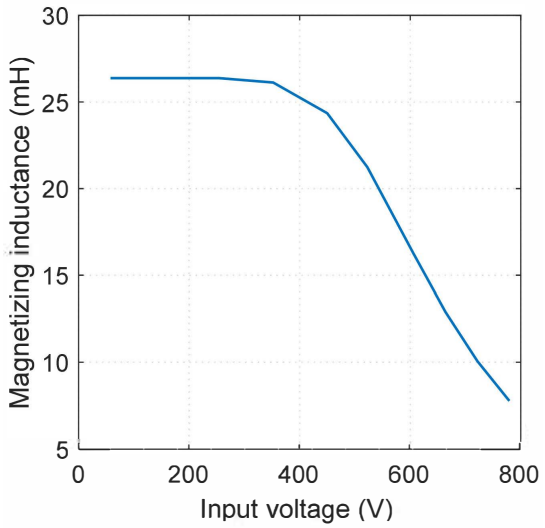

Figure 5. Magnetizing inductance.

The line segment from Sanjiaotang station to Zhongyangling station was chosen as the programming target. The data for the train running under ATO were collected and analyzed. The travel time between the two stations was 110 s, and the distance between the two stations was 1463 m. The speed limits and slopes are shown in Figure 6. The maximum sustainable tractive force and braking force generated by the propulsion system are shown in Figure 7. The ECM of the TM is solved by MATLAB/Simulink. Using the efficiency calculation method proposed in Section 2, the efficiency $\eta_m(\omega_m, P_2)$ and $\eta_m(v, F_t)$ can be obtained, as shown in Figure 8.

As shown in Figure 8a, the maximum efficiency of the motor is 0.87, and the mean value is 0.81. When the output power of the motor is low, the efficiency of the propulsion system is extremely low. In the low-to-medium speed range, the motor efficiency increases with the output power. In the high-speed range, as the speed increases, the efficiency slowly decreases because the motor tends to saturate. Figure 8b shows the efficiency contour of the high-efficiency interval; the corresponding efficiency values are {0.8, 0.81, 0.82, 0.83, 0.84, 0.85, 0.86}. Figure 8c shows the efficiency contour of the low-tractive force interval; the corresponding efficiency values are {0.1, 0.2, 0.3, 0.4, 0.5, 0.6, 0.7, 0.8}. It can be seen from Figure 8b,c that as the train speed or traction force increases, the

traction efficiency gradually increases. When the train operates in a low-traction zone, the traction efficiency falls sharply.

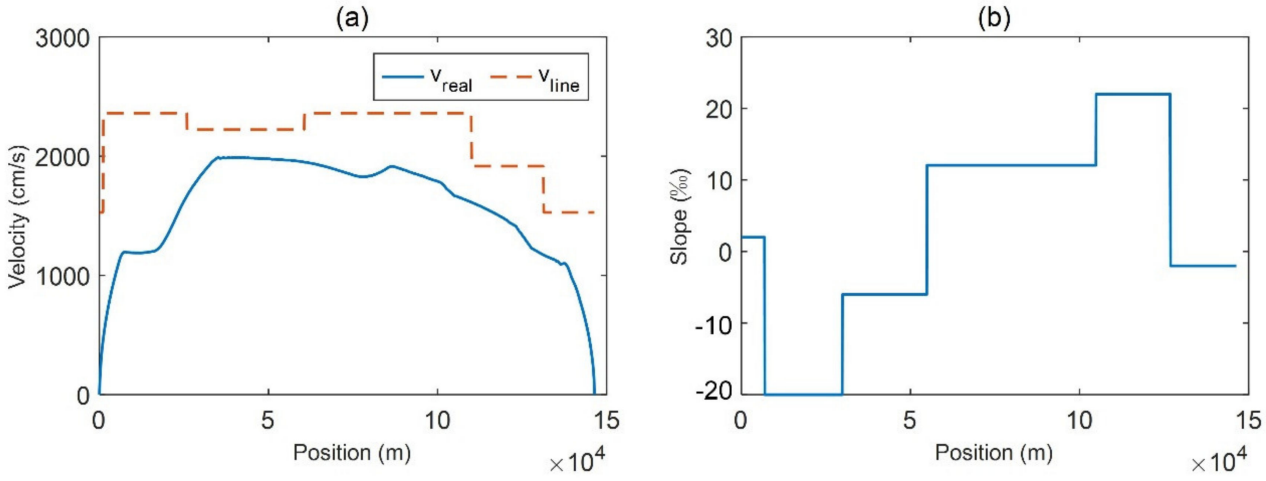

Figure 6. Line speed limit and slope: (**a**) line limit and actual running speed; (**b**) slope of the line.

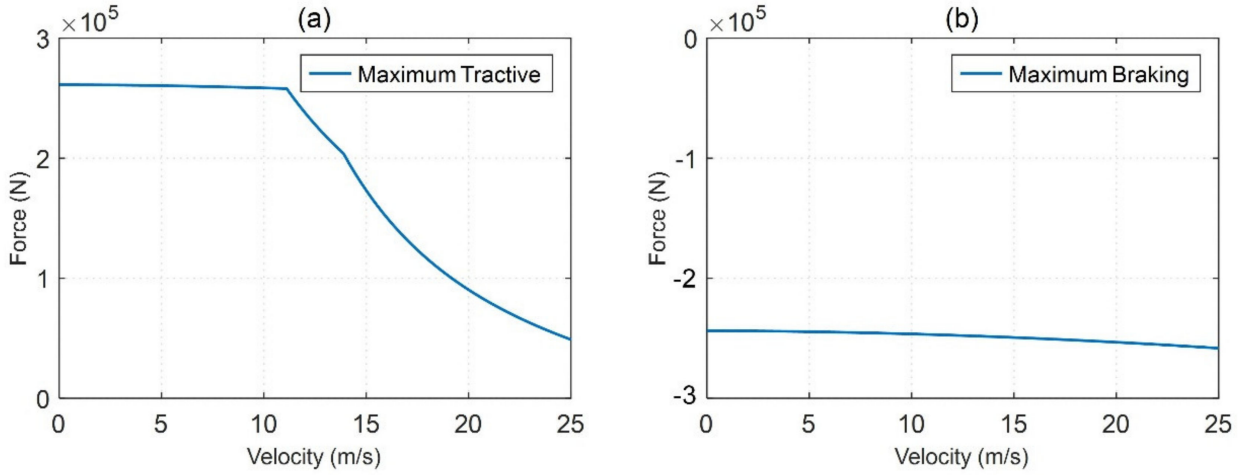

Figure 7. Maximum force generated by propulsion system: (**a**) maximum tractive force; (**b**) maximum braking force.

Based on the DP method proposed in Section 3, an optimal speed curve-solving program was written in MATLAB. The maximum value of the state variable x_k was set to $\begin{bmatrix} L & V_{max} \end{bmatrix}$, and discretized according to the step sizes of ds and dv. To study the influence of different steps, four experiments were conducted. The parameter settings and solution results of the four experiments are compared in Table 2 and Figure 9. As shown in Table 2, as the step decreases, the energy consumption value corresponding to the speed curve gradually decreases, but the runtime increases significantly. In Experiment one, because ds is large, the energy consumption value of the speed curve obtained by the solution is also large. The position error of the endpoint is also large. A significant negative position error at the *Nth* step means that the train has not yet reached the target stopping point at the end of the decision stage. However, Experiment one requires the shortest solution time, and it only takes 16 min to complete the solution to the speed curve. In Experiments two and three, the position and velocity errors at the *Nth* step are within acceptable ranges. The energy consumption value is also low, but the runtime increases accordingly. In Experiment four, as the step size is shortened further, the time required to solve the problem is significantly increased, and the energy consumption value decreases less. The position error at the endpoint is positive, which means that the train will run

to a position beyond the target stopping point. It can be seen that when discretizing the state space, an appropriate step size should be used. In Figure 9, it can be seen that the maximum operating speed of Experiments one to four is decreasing, and the traction time is also decreasing correspondingly.

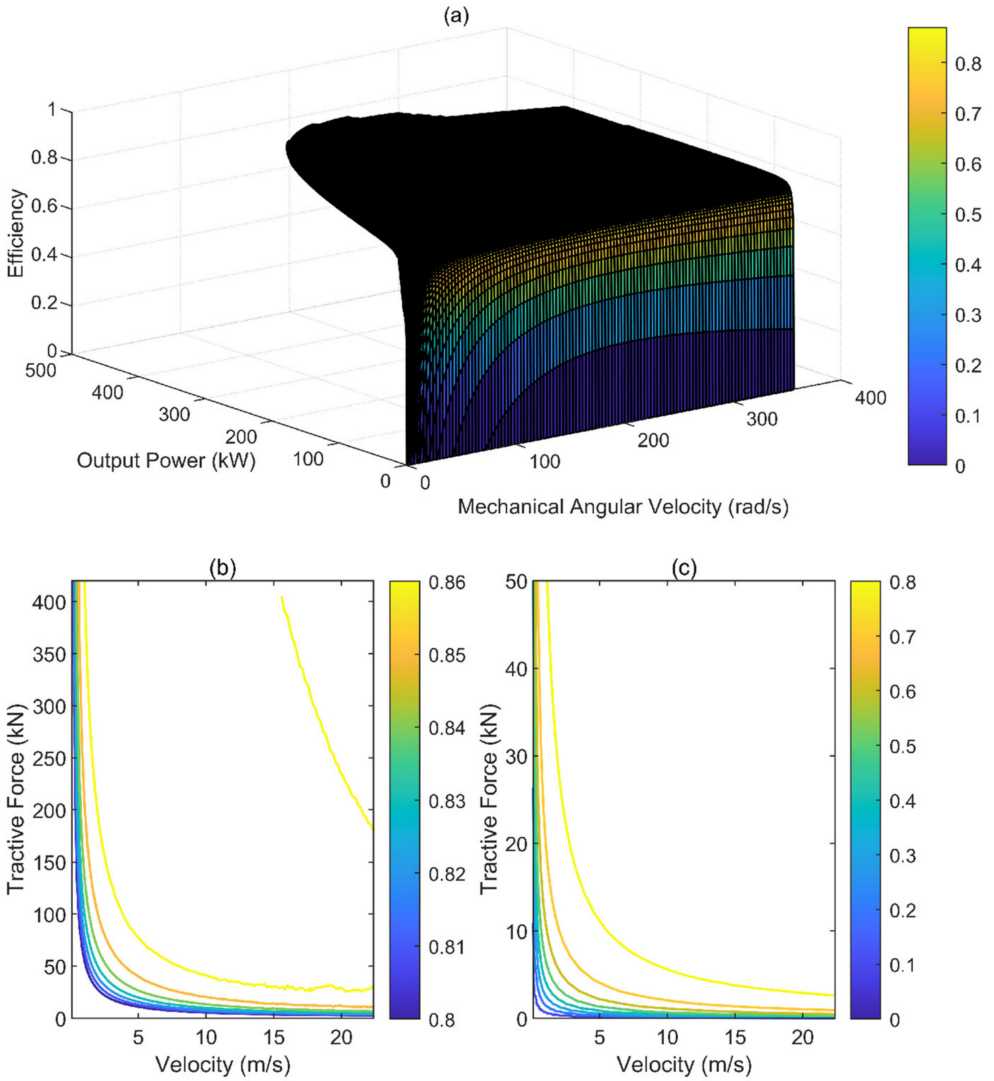

Figure 8. Demonstration of the efficiency at different work points: (**a**) efficiency of one traction motor at different frequencies and torques; (**b**) efficiency contours in the high-efficiency range; (**c**) efficiency contours in the low-traction-force range.

Table 2. Influence of state step length on the velocity curve solution.

Experiment ID	*ds* (m)	*dv* (m/s)	$S_N - L$ (M)	V_N (M/S)	Energy Consumption (J)	Runtime (Minutes)
1	2	1	−2.77	0.396	6.15×10^7	16
2	1	1	−0.34	0.55	4.96×10^7	48
3	1	0.5	−0.4	0	4.29×10^7	205
4	0.5	0.5	1.26	0	4.00×10^7	2238

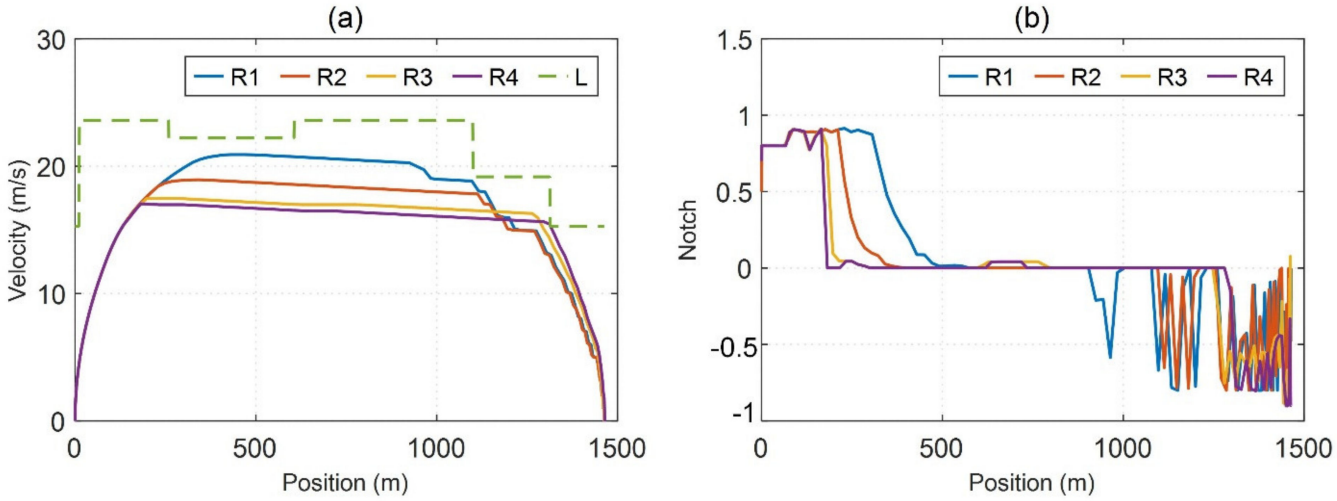

Figure 9. Comparison of the DP solution results with different state variable steps: (**a**) speed curve; (**b**) control notch curve.

The energy consumed by the actual operating speed curve is solved using the proposed energy consumption calculation method to obtain an energy consumption value of 6.28×10^7 J. Comparing the actual operating speed curve with Experiment two, it can be seen that the proposed optimization method reduces the energy consumption by 20% compared with the current train operation curve.

To analyze the performance of the DP algorithm, the fuzzy GA method proposed by Li et al. [24] was selected for comparison. Owing to the short distance between the two subway stations, the driving style of acceleration–cruising–coasting–braking was selected for optimization. The optimization vector comprising the decision variables is $x = \begin{bmatrix} x_t & x_{cr} & x_{co} & x_b \end{bmatrix}$, where $x_t = \frac{a_t}{a_{max}}$, $x_{cr} = \frac{v_{cr}}{v_{max}}$, $x_{co} = \frac{v_{co}}{v_{cr}}$, and $x_b = \frac{a_b}{a_{min}}$. a_t is the acceleration; v_{cr} is the cruising speed; v_{co} is the coasting end speed; and a_b is the deceleration of the braking stage. The solution process is shown in Figure 10. In Figure 10, it can be seen that as the algebra increases, the fitness value gradually decreases and finally converges to a minimum fitness value, and the optimal individual produced by the genetic algorithm is $x = \begin{bmatrix} 0.8476 & 0.8493 & 0.9766 & 0.7917 \end{bmatrix}$. The runtime is 3.944 s, and the energy consumption is 4.0814×10^7 J. As the four fixed driving styles are set and the number of optimization variables is reduced, the time to solve the GA is significantly reduced. The energy consumption is also very close to that of Experiment four.

Figure 11 compares the DP algorithm, GA, and actual operation, where A represents the actual operating curve; GA represents the speed profile solved by the GA; R4 represents the experimental four curves; and L represents the line speed limit. It can be seen from the figure that the maximum speed of the actual operating curve is greater than the energy consumption of DP and GA. The actual operating curve has multiple tractions during the running process, which increases the total traction time. Furthermore, owing to the low efficiency of the TM at low output power or low traction force, the energy consumption is further increased. Comparing the curves of GA and DP, it is clear that the velocity curves obtained using the two methods are close. However, the control notch of the train differs significantly during the acceleration phase. The traction level required by the GA in the final stage of acceleration exceeds both the maximum level of the train and the maximum traction force that the traction system can output. This is because the GA only considers the fixed maximum acceleration value a_{max} when considering the variable constraints. The actual maximum acceleration value of the train will decrease as the train speed increases, as shown in Figure 7a; thus, the speed curve solved by the GA does not satisfy the constraints of the traction system. As the DP algorithm updates the maximum and minimum traction force that the following cars can output at the corresponding speed at each decision stage, the control level of the DP algorithm can satisfy the tractive capacity constraints of the train.

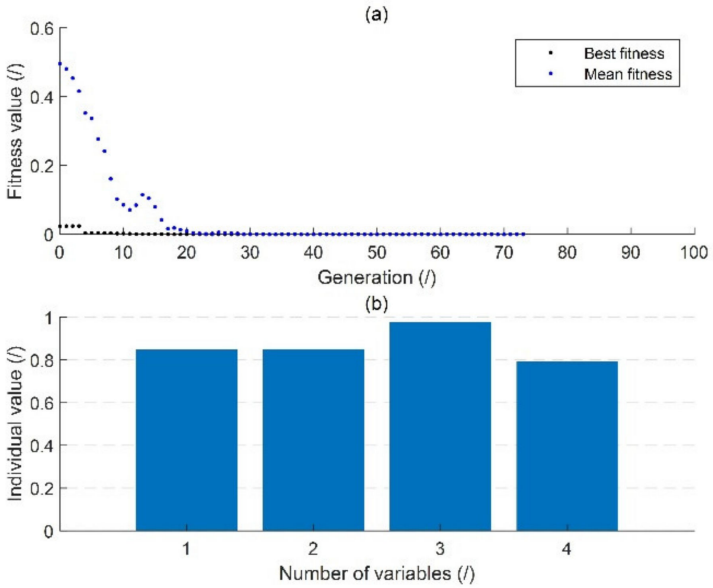

Figure 10. Solving process of the genetic algorithm: (**a**) fitness value; (**b**) best individual.

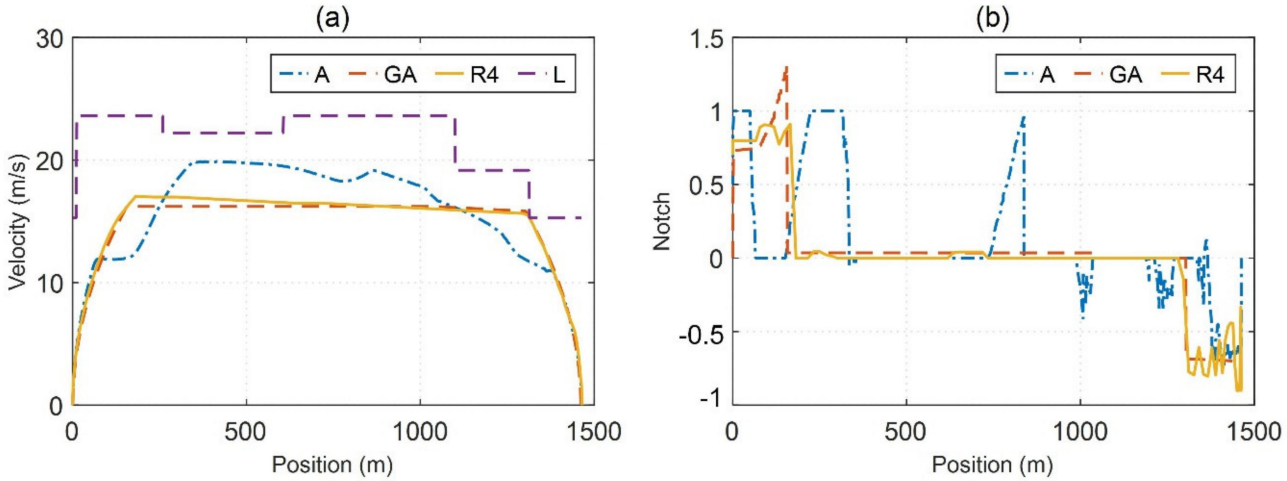

Figure 11. Comparison of different algorithms: (**a**) speed curve; (**b**) control notch curve.

5. Conclusions

Traction energy consumption accounts for a large proportion of the total energy consumption of subway operations. Optimizing the operating speed curve of trains without adding new energy storage facilities is of great significance to the energy-saving operation of railways.

This study carefully considered the model of the train traction propulsion system and the changes in motor efficiency at different operating points, which resulted in an estimated traction energy consumption that was closer to the actual value. Using the evaluated traction energy, an optimal speed profile planning method based on DP was proposed in this paper. The proposed method considers the constraints of the line speed limit, passenger comfort, and travel time. Through the simulation analysis of an actual subway line, it is found that the proposed speed curve optimization method can reduce the energy consumption of the train under the given running time constraint. Further, by comparing different discrete step sizes in the state space, it is found that as the step size decreases, the energy consumption of the solved speed curve gradually decreases, and the solution time drastically increases. Therefore, it is necessary to select an appropriate discrete step size in the state space. Through the comparative test with the GA, it is seen

that the advantage of the DP algorithm is that it can search for a lower energy consumption curve and satisfy the complex constraints of the line speed limit and the train traction capacity. However, the disadvantage is that the search time is too long. As the GA sets the heuristic rules of driving style, its solution time is significantly less. However, the disadvantage of the GA is that it cannot handle the constraints of train traction capacity and line speed limit changes. Solving the optimal speed curve using the proposed method offline and programming the onboard controller of the train according to the optimal speed curve enables the train to be driven with greater energy efficiency.

The limitation of the proposed method is that as the scale of the state space increases, the solution time reaches the order of hours, which cannot support the online adjustment of train speed curves. Future work will focus on optimizing the solution algorithm and shortening the solution time to support the online adjustment of the speed curve. In addition, calculation methods for train traction energy consumption and speed curve optimization will also be investigated for subway lines with energy storage systems.

Author Contributions: Conceptualization, T.T.; formal analysis, Z.W. and T.T.; investigation, Z.W.; methodology, Z.W. and C.G.; resources, C.G.; supervision, C.G.; writing—original draft, Z.W. All authors have read and agreed to the published version of the manuscript.

Funding: This research was funded by the Beijing Postdoctoral Research Foundation (No. 2020-22-091).

Institutional Review Board Statement: Not applicable.

Informed Consent Statement: Not applicable.

Data Availability Statement: Not applicable.

Acknowledgments: We wish to thank KINGWAY RAIL for providing the relevant train parameters.

Conflicts of Interest: The authors declare no conflict of interest.

References

1. European Environmental Agency. Specific CO_2 Emissions Per Passenger-Km and Per Mode of Transport in Europe. 1995–2011. Available online: https://www.eea.europa.eu/data-and-maps/figures/specific-co2-emissions-per-passenger-3 (accessed on 1 July 2021).
2. International Energy Agency & International Union of Railways. Railway Handbook 2017: Energy Consumption and CO_2 Emissions. 2017. Available online: https://uic.org/IMG/pdf/handbook_iea-uic_2017_web3.pdf (accessed on 1 July 2021).
3. Liu, Z.; Qin, C.; Zhang, Y. The energy-environment efficiency of road and railway sectors in China: Evidence from the provincial level. *Ecol. Indic.* **2016**, *69*, 559–570. [CrossRef]
4. Giordano, D.; Clarkson, P.; Gamacho, F.; van den Brom, H.E.; Donadio, L.; Fernandez-Cardador, A.; Spalvieri, C.; Gallo, D.; Istrate, D.; Laporte, A.D.; et al. Accurate measurements of energy, efficiency and power quality in the electric railway system. In Proceedings of the 2018 Conference on Precision Electromagnetic Measurements, Paris, France, 8–13 July 2018.
5. Giordano, D.; Davide, S. MyRailS: Metrology for Smart Energy Management in Railway System. 2019. Available online: https://myrails.it/wp-content/uploads/2020/05/02_The_European_Research_Project_MyRailS_D.Giordano.pdf (accessed on 1 July 2021).
6. Gunselmann, W. Technologies for increased energy efficiency in railway systems. In Proceedings of the 2005 European Conference on Power Electronics and Applications, Dresden, Germany, 11–14 September 2005.
7. Liu, R.R.; Golovitcher, I.M. Energy-efficient operation of rail vehicles. *Transp. Res. Part A Policy Pract.* **2003**, *37*, 917–932. [CrossRef]
8. He, D.; Yang, Y.; Chen, Y.; Deng, J.; Shan, S.; Liu, J.; Li, X. An integrated optimization model of metro energy consumption based on regenerative energy and passenger transfer. *Appl. Energy* **2020**, *264*, 114770. [CrossRef]
9. González-Gil, A.; Palacin, R.; Batty, P.; Powell, J.P. A systems approach to reduce urban rail energy consumption. *Energy Convers. Manag.* **2014**, *80*, 509–524. [CrossRef]
10. Rind, S.J.; Ren, Y.; Hu, Y.; Wang, J.; Jiang, L. Configurations and control of traction motors for electric vehicles: A review. *Chin. J. Electr. Eng.* **2017**, *3*, 1–17. [CrossRef]
11. Delle Femine, A.; Gallo, D.; Landi, C.; Luiso, M. Discussion on DC and AC power quality assessment in railway traction supply systems. In Proceedings of the 2019 IEEE International Instrumentation and Measurement Technology Conference, Auckland, New Zealand, 20–23 May 2019; pp. 1–6. [CrossRef]
12. Delle Femine, A.; Gallo, D.; Giordano, D.; Landi, C.; Luiso, M.; Signorino, D. Power quality assessment in railway traction supply systems. *IEEE Trans. Instrum. Meas.* **2020**, *69*, 2355–2366. [CrossRef]
13. Alfieri, L.; Battistelli, L.; Pagano, M. Energy efficiency strategies for railway application: Alternative solutions applied to a real case study. *IET Electr. Syst. Transp.* **2018**, *8*, 122–129. [CrossRef]

14. Zhao, N.; Roberts, C.; Hillmansen, S.; Tian, Z.; Weston, P.; Chen, L. An integrated metro operation optimization to minimize energy consumption. *Transp. Res. Part C Emerg. Technol.* **2017**, *75*, 168–182. [CrossRef]
15. Huang, Y.; Yang, L.; Tang, T.; Gao, Z.; Cao, F. Joint train scheduling optimization with service quality and energy efficiency in urban rail transit networks. *Energy* **2017**, *138*, 1124–1147. [CrossRef]
16. De Martinis, V.; Corman, F. Data-driven perspectives for energy efficient operations in railway systems: Current practices and future opportunities. *Transp. Res. Part C Emerg. Technol.* **2018**, *95*, 679–697. [CrossRef]
17. Yang, X.; Li, X.; Ning, B.; Tang, T. A survey on energy-efficient train operation for urban rail transit. *IEEE Trans. Intell. Transp.* **2016**, *17*, 2–13. [CrossRef]
18. Zarifyan, A.; Grebennikov, N.; Talakhadze, T.; Romanchenko, N.; Shapshal, A. Increasing the energy efficiency of rail vehicles equipped with a multi-motor electrical traction drive. In Proceedings of the 2019 26th International Workshop on Electric Drives: Improvement in Efficiency of Electric Drives (IWED), Moscow, Russia, 1 January–2 February 2019.
19. Liubarskyi, B.; Demydov, A.; Yeritsyan, B.; Nuriiev, R.; Iakunin, D. Determining electrical losses of the traction drive of electric train based on a synchronous motor with excitation from permanent magnets. *East. Eur. J. Enterp. Technol.* **2018**, *2*, 29–39. [CrossRef]
20. Serhiy, M.; Artem, B.; Danylo, P. Searching of the optimum configuration of the traction electric transmission of the shunting locomotive. In Proceedings of the 2019 IEEE International Conference on Modern Electrical and Energy Systems (MEES), Kremenchuk, Ukraine, 23–25 September 2019.
21. Ghavihaa, N.; Javier, C.; Markus, B.; Erik, D. Review of application of energy storage devices in railway transportation. *Energy Procedia* **2017**, *105*, 4561–4568. [CrossRef]
22. Yang, X.; Chen, A.; Wu, J.; Gao, Z.; Tang, T. An energy-efficient rescheduling approach under delay perturbations for metro systems. *Transportmetrica* **2019**, *7*, 386–400. [CrossRef]
23. Tian, Z.; Zhao, N.; Hillmansen, S.; Roberts, C.; Dowens, T.; Kerr, C. SmartDrive: Traction energy optimization and applications in rail systems. *IEEE Trans. Intell. Transp.* **2019**, *20*, 2764–2773. [CrossRef]
24. Li, Z.; Chen, L.; Roberts, C.; Zhao, N. Dynamic trajectory optimization design for railway driver advisory system. *IEEE Intell. Transp. Syst. Mag.* **2018**, *10*, 121–132. [CrossRef]
25. Wang, P.; Goverde, R.M.P. Multi-train trajectory optimization for energy efficiency and delay recovery on single-track railway lines. *Transp. Res. Part B Methodol.* **2017**, *105*, 340–361. [CrossRef]
26. Huang, K.; Wu, J.; Yang, X.; Gao, Z.; Liu, F.; Zhu, Y. Discrete train speed profile optimization for urban rail transit: A data-driven model and integrated algorithms based on machine learning. *J. Adv. Transport.* **2019**, *2019*, 7258986. [CrossRef]
27. Ghaviha, N.; Bohlin, M.; Holmberg, C.; Dahlquist, E.; Skoglund, R.; Jonasson, D. A driver advisory system with dynamic losses for passenger electric multiple units. *Transp. Res. Part C Emerg. Technol.* **2017**, *85*, 111–130. [CrossRef]
28. Kristianingtyas, K.D.; Miyatake, M. Design of optimal train speed profile for PMSM railway traction system using dynamic programming with MTPA control method. In *Urban Rail Transit*; Springer: Berlin/Heidelberg, Germany, 2021; pp. 291–309. [CrossRef]
29. Liu, F.; Wu, J.; Zhang, Z.; Lu, H.; Li, K. Operation optimisation of urban rail transit train base on energy saving. *Int. J. Mater. Struct. Integr.* **2018**, *12*, 1–16. [CrossRef]